Molecular properties of soil organic matter in dark buried colluvium from South Germany show abundance of fire residues from Early Neolithic vegetation clearance and slash and burn agriculture

JOERI KAAL[1] AND SONJA MAILÄNDER[2]

[1] *Pyrolyscience, Santiago de Compostela, Spain*
[2] *Institute of Geography, University of Stuttgart, Germany*

Compiled January 10, 2019

Geoarchaeological surveys in South Germany (Nördlinger Ries area) showed continuous presence of human occupations since the Palaeolithic and remarkable colluvial soils containing dark buried layers dated to the Neolithic. Here we discuss molecular properties of soil organic matter (SOM) from three of these colluvia by Py-GC-MS. The pyrolysis products could be ascribed to four different SOM components: labile SOM (fresh lignin and polysaccharides), a recalcitrant aliphatic fraction, degraded/secondary SOM (including chitin and degraded carbohydrates) and pyrogenic SOM (Black C, from palaeofires). The Black C was recognised unambiguously from the full range of diagnostic compounds, i.e. abundant polycyclic aromatic hydrocarbons (PAHs) such as naphthalenes, biphenyl, fluorene, phenanthrene, anthracene and pyrene, and N-containing compounds such as benzonitrile, (iso)quinoline and naphthalene carbonitriles. Black soil layers generally contained larger proportions of pyrogenic material but SOM dynamics of these soils seem controlled by intense degradation, eliminating most components of fresh plant material and producing newly-formed degraded SOM (including chitin from fungi and/or arthropods) and a relative accumulation of aliphatic SOM. Nonetheless, the black colour of the Neolithic soil layers is clearly caused by the strong pigmentation of fire residues and reflects a series of (forest) fire events ca. 6000–7000 cal BP. This study shows the potential of Py-GC-MS to identify pyrogenic SOM and simultaneously identify the processes that control SOM dynamics in prehistorical anthropogenic colluvium.

1. INTRODUCTION

Pyrolysis-GC-MS is increasingly used for Black C identification and characterization in archaeological sites but also off-site anthropogenic dark earths such as worldwide *Terra Preta* deposits and colluvial deposits, despite the potential difficulties in distinguishing artificial thermal modifications (during analytical pyrolysis) and the "natural" thermal impact by fire. While many of the major pyrolysis products of Black C, e.g. benzene, toluene, C_2-benzenes, pyridine and PAHs, are not specific of Black C, they tend to be enriched in Black C-rich soil and, if the chromatogram quality is optimized, accompanying compounds such as benzene carbonitriles or naphthalene carbonitriles may allow for a definitive identification of the pyrogenic SOM signal.

Excavations and geomorphological research in the study area by Sonja Mailänder and her colleagues Prof. Dr. Wolf-Dieter Blümel and Dr. Joachim Eberle showed a series of partially black-coloured colluvial deposits that formed the basis of a landscape reconstruction exercise, i.e. the PhD research of Sonja Mailänder. For details of this research, the study area, and the deposits we examined by analytical pyrolysis, please refer to Mailänder et al. (2010, 2011).

Aiming to elucidate soil formation processes and to seek for indications of human activities (anthropogenic remains and land use strategies), we performed Py-GC-MS to the SOM from the three soil profiles, with special interest in the nature of the SOM in the buried dark layers.

2. MATERIALS AND METHODS

A. Study area

The study area is located nearby the Ipf Mountain (Nördlinger Ries, South Germany, 80 km east of Stuttgart), which is on the border of crater that formed upon a Miocene meteorite impact 15 million years ago (Figures 1 and 2).

Figure 3 shows the colluvial deposits (taken from a pipeline trench), samples analysed, and radiocarbon dates. Profile A is located to the north-east of the Ipf hill in the upper reaches of the Goldbach Valley. This valley has no watercourse anymore and is used as grassland and grazed by cattle. In the pipeline trench the black layer (A4), which was covered by colluvial deposits, appeared in the deepest part of the depression and lashed out to the left and to the right. A calcareous-rich layer was found

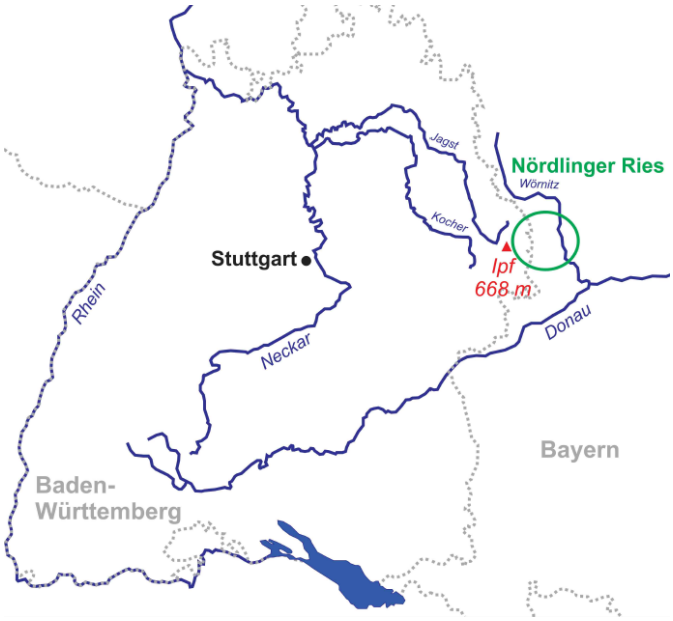

Fig. 1. The study area is situated in southwest Germany at the western border of the Nördlinger Ries, which is a crater formed by a Miocene meteorite impact 15 Million years ago.

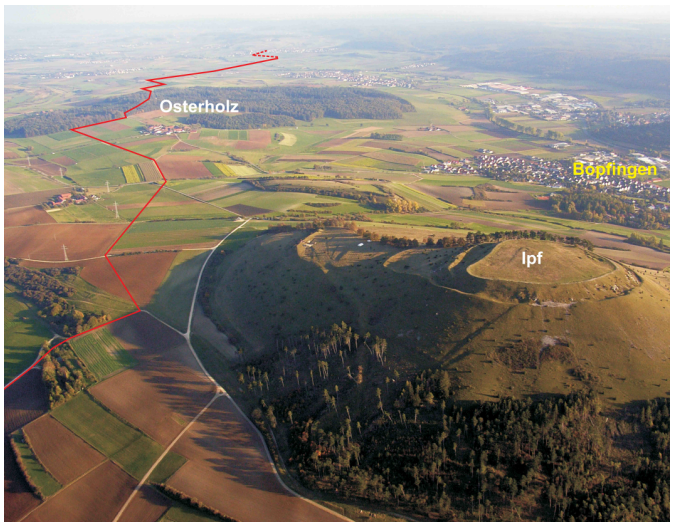

Fig. 2. This aerial picture shows the mountain Ipf near the city of Bopfingen. The red line marks the course oft the pipeline ditch, which was investigated in the years 2006 and 2007 (Foto: S. Mailänder, Oktober 2007).

underneath layer A4 (A5). The geological substrate is composed of the Upper Aalenian (Aalenian 2, al2E, former Brown Jurassic).

Profile B is situated further east within the outer ring of the Ries crater, nearly on top of a small depression, which runs to the Goldbach Valley from the west. Today this area is used for agriculture. The underlying bedrock is a dislocated Upper Jurassic megablock. In profile B a dark layer (B6) was found as well, at the deepest part of the depression lashing out to the slopes and covered by colluvial deposits. In the position of the investigated profile in the pipeline trench, a small pit-like structure appeared underneath (B7).

Profile C was studied on the south-facing, gently tapered slope of the Eger Valley, also within the megablock zone of the crater. Here the basement is built of Bunte Breccia that is a product of the meteorite impact. It consists of multicoloured chaotically mixed rock fragments, which originate from different bedrock formations. On top of a very clayey black horizon (C6), poor in coarse particles, two further dark layers (C5 and C4) are found, which contained many pieces of Upper Jurassic limestone.

B. HF treatment

Minerals that catalyze secondary rearrangements during pyrolysis were eliminated by HF treatment. Briefly, 2.0 g of sample were transferred into 50 ml centrifuge tubes and 10 ml of 1 M HCl were added repeatedly to remove carbonates. After the reaction was completed, H_2O was added until the 25 ml mark and the resulting suspension was agitated, centrifuged (2500 rpm for 10 min) and the supernatant discarded. Next, 2 % HF solution was added until the 25 ml mark and shaken for 24 hrs, followed by centrifugation and decantation of the supernatant. This HF treatment was repeated 5 times, after which the procedure was executed three times with H2O to wash away the acid and silicates. Finally, the residue was dried at 35 ºC.

C. Pyrolysis-GC-MS

Pyrolysis-GC-MS was performed using a Pt filament coil probe resistive heating pyrolyzer (Pyroprobe 5000) from CDS Analytical Inc (Oxford, USA). The pyrolysis interface was connected to a 6890 GC and 5975 MSD from Agilent Technologies (Palo Alto, USA). Approximately 1 mg of sample (HF-treated residue) was embedded in fire-polished quartz tubes using glass wool. Pyrolysis was performed at 750 ºC (*750 ºC setpoint temperature is approximately 670 ºC real pyrolysis temperature which is still very high, but found ideal for Black Carbon characterization by Kaal et al. 2009*) for 10 s at a heating rate of 10 °C ms^{-1}. The pyrolysis interface and GC inlet were set at 325 °C. The GC oven was heated from 50 to 325 °C at 20 °C min^{-1} and held isothermal for 5 min. The GC-MS transfer line was held at 325 °C, the ion source (electron ionisation mode, 70 eV) at 230 °C and the quadrupole detector at 150 °C. The GC was equipped with a (non-polar) HP-5MS 5% phenyl, 95% dimethylpolysiloxane column (ca. 30 m x 0.25 mm i.d.; film thickness 0.25m). Helium was used as carrier gas (constant flow, 1 ml min^{-1}). Two replicates were obtained for each sample. The ca. 50 largest peaks of the total ion current of each pyrolysis chromatogram were listed, giving rise to a compound list of 114 pyrolysis products. The relative proportions of the pyrolysis products were calculated from the peak area of their dominant and/or characteristic mass fragments. Relative proportions are expressed as the percentage of total quantified peak area (% TQPA). Two replicates were obtained for each sample.

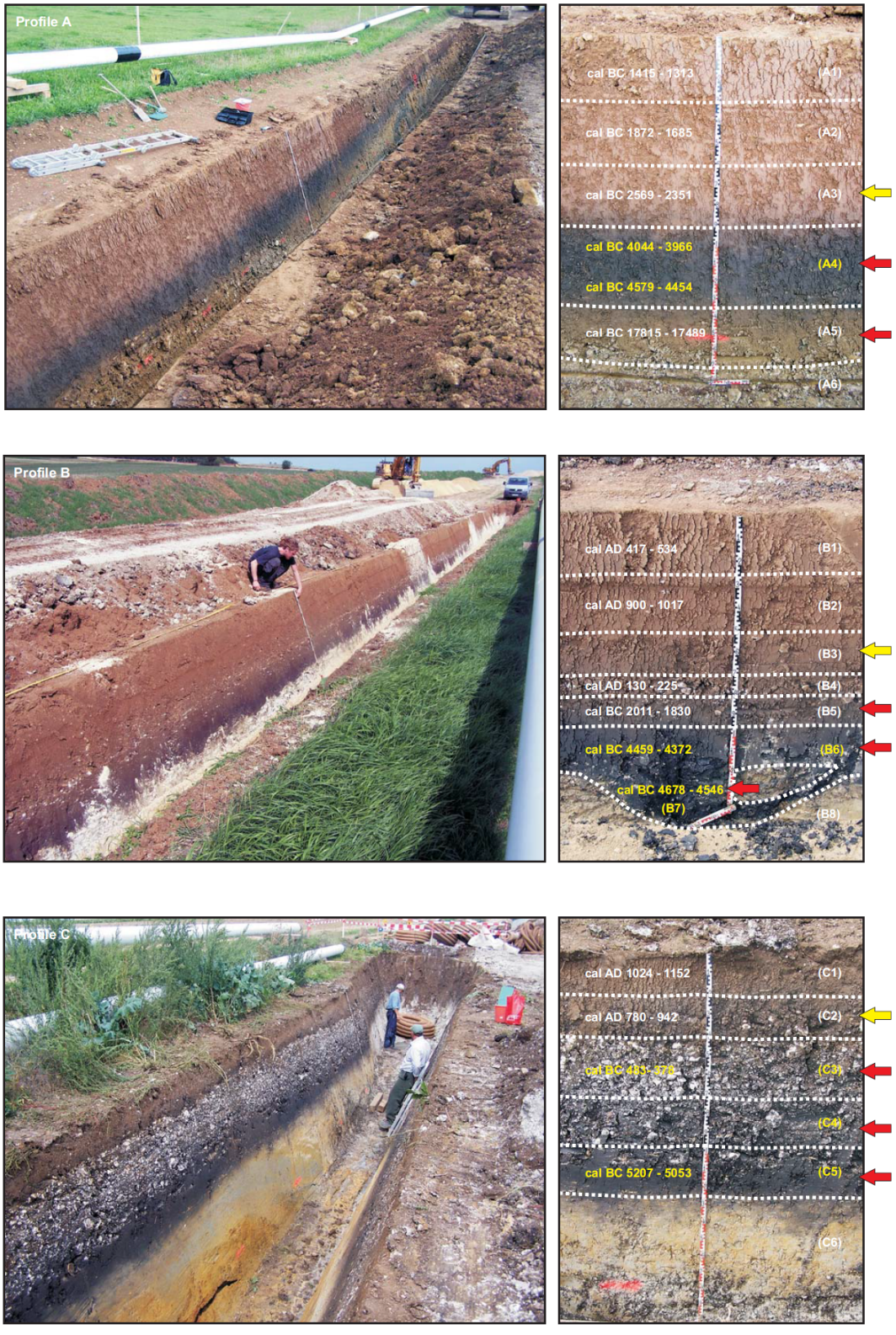

Fig. 3. Photographs from the colluvial deposits, taken from a pipeline ditch. Samples from profile A, B and C that were analysed by Py-GC-MS are marked with arrows.

3. RESULTS AND DISCUSSION

A. Py-GC-MS products and source allocation

The list of compounds is provided in Table 1 at the bottom of this article. The pyrolysis products were grouped based on chemical structure and/or most likely origin: The markers of carbohydrates are 3/2-furaldehyde, 5-methyl-2-furaldehyde, 4-hydroxy-5,6-dihydro-(2*H*)-pyran-2-one, dianhydrorhamnose, levoglucosenone and levoglucosan. Of these compounds, levoglucosan, dianhydrorhamnose and 4-hydroxy-5,6-dihydro-(2*H*)-pyran-2-one originate mainly from relatively intact polysaccharides while levoglucosenone and the furfurals originate from degraded carbohydrates, even though there is no strict division between these two subgroups (intact polysaccharides also produce furfurals upon pyrolysis). An unidentified compound producing base ion m/z 116 was grouped here as it is possibly an indication of moss-derived carbohydrate (Schellekens et al., 2011), and was correlated to the three markers of intact polysaccharide (3x (P<0.001). The seven carbohydrate products combined account for 12 ± 4 % of TQPA (Fig. 4a). This proportion decreases with depth in the three soils, which may be explained by preferential carbohydrate decomposition with time. In profiles B and C, the relative proportion of intact carbohydrate markers declines with depth, reflecting carbohydrate degradation. However, in profile A, sample A5, which is the only Late-Pleistocene/Early Holocene sample of the present study, produced a relatively large proportion of intact polysaccharide markers, probably because this layer formed under conditions with low microbial activity (cold and dry).

Pyrolysis products containing one or more atoms of N (N-containing compounds) are abundant, i.e. 23 ± 3 % of TQPA (Fig. 4b). These compounds have a diverse origin, and a VARCLUS cluster analysis using Tanagra software was performed to arrange them into subgroups (not shown). Two main clusters were obtained, accounting for 85 ± 4 % of total N-containing pyrolysis products. One cluster consists of (in decreasing order of cluster correlation coefficient) acetamide, C_1-pyrrole, a compound with base ion (m/z 94), benzeneacetonitrile, trianhydro-2-acetamido-2-deoxyglucose, 2,5-diketopiperazine, C_1-pyridine, a compound with base ion m/z 109, and m/z 66 and m/z 80 as daughter ions of two co-eluting isomers), indole and pyrrole. The compounds with m/z 94, m/z 109 and trianhydro-2-acetamido-2-deoxyglucose are markers of the *N*-acetylglucosamine-based biopolymer chitin, which occurs in invertebrate/arthropod exoskeleta, fungi cell walls and also in molluscs. The diketopiperazine has been identified in pyrolyzates of chitin-entangled protein, and the other products can also be produced by chitin but are less specific. Therefore, the compounds in this cluster are thought to originate primarily from chitin. Chitin seems to be present in all samples (Fig. 4b). Its proportion declines with depth in profiles B and C. An unidentified compound with fragment ions m/z 59, 114 and 204, which could correspond to 1,6-dianhydro-2-acetamido-2-desoxyglucose, was identified in an isolated snail shell fragment from sample A4 (not shown). This compound, which could be a marker of mollusc chitin, was not found in the HF-treated samples. Nonetheless, it is difficult to decide on the source organism of the chitin markers. We believe that they are mainly arthropod-derived and/or fungal, either way being an indication of biological recycling of plant-derived SOM. The second cluster consists of two naphthalene carbonitrile isomers, benzonitrile, *N*-methylpyrrole, C_1-benzonitrile and pyridine. The naphthalene carbonitriles (or naphthonitriles) and benzonitriles are markers of pyrogenic N (Kaal et al., 2009), and pyridine is a less-specific of it (e.g. Kaal and Rumpel, 2009). The depth trend of this pyrogenic N (or Black N; Knicker, 2010) is discussed below. The position of the N-methylpyrrole in this cluster cannot be explained (it is an unlikely product of pyrogenic material). Furthermore, we identified a set of phthalimides (three compounds), which we think are also markers of pyrogenic N. Diketodipyrrole (a dimerization product of protein pyrolysis), C_{16}- and C_{18}-alkylamide, and C_{16}- and C_{18}-alkylnitrile, were also detected but not associated with one of the aforementioned clusters.

In the present study, the guaiacyl- and syringyl-based pyrolysis products of lignin were scarce (0.5 ± 0.2 % of TQPA). Also, only guaiacol and 4-vinylguaiacol were detected. This implies that either lignin was not a significant source of the SOM or that it was profoundly remediated. Lignin is enriched in the SOM of the Early Holocene sample A5 (confirming the preservation of some lignocellulosic source) while it decreases with depth in profiles B and C, probably because of decay (Fig. 4c).

Considering the presence of lignin as well as pyrogenic matter and abundant degraded and secondary biomass, which all produce phenols upon pyrolysis, the phenols (4.1 ± 0.7 % of TQPA) cannot be ascribed to a specific SOM component. From the relative proportion of phenols in profile C (Fig. 4d), which shows a similar trend to that of the lignin markers, it may be concluded that the phenols in that soil originate primarily from degraded lignin. Analogously, in profiles A and B the phenols may be derived mainly from N-containing proteinaceous biomass.

Monocyclic aromatic hydrocarbons (MAHs) account for 24 ± 2 % of TQPA. Toluene is the most abundant product, followed by benzene. These two compounds exhibit inverse depth trends (Fig. 4e). While toluene is correlated to the products of chitin (r^2=0.31, P<0.05), benzene is correlated to pyrogenic N (r^2=0.48, P<0.001). This behaviour may be expected from soil samples with large proportions of both proteinaceous biomass and pyrogenic matter. The other MAHs (xylenes and ethylbenzene) may have diverse origins, so that they cannot be allocated to a specific SOM component.

Polycyclic aromatic hydrocarbons (PAHs) account for 3.4 ± 0.7 % of TQPA. Here, the main source of these compounds is pyrogenic matter, i.e. Black C. PAHs increase with depth in soils B and C, but not in soil A (Fig. 4f).

The group of methylene chain compounds (MCC) includes homologous series of *n*-alkanes (C_{10}-C_{33}), *n*-alkenes (C_{10}-C_{31}), *n*-fatty acids (C_{16} and C_{18}) and 2-methylketones (C_{23}, C_{25}, C_{27} and C_{29}), in addition to prist-1-ene. Combined, these compounds account for 34 ± 5 % of TQPA (Fig. 4g). The vast majority of this group can be ascribed to *n*-alkane/*n*-alkene pairs (30 ± 5 % of TQPA). The increase with depth in all soils can be explained by the resistance of aliphatic material during SOM degradation, in this case their relative preservation compared to mainly carbohydrates but also compared to chitin.

Other compounds (3.1 ± 1.4 % of TQPA) include methyliodine (m)/(z 142 and 127; 1.2 ± 0.7 % of TQPA), which is not frequently found in SOM pyroyzates (Fig. 4h). A possible source of this compound is halogenation: these clay-rich soils release significant amounts of I upon weathering which, in combination with the high microbial/biological activity, forms organo-iodine complexes through biotic halogenation. We checked for the presence of methylbromine (which should be formed through the same process; Martínez-Cortizas et al., 2016), and we identified this compound as well (m/z 94, 96). Quantification of Me-Br, not presented in the Appendix because it was not recognised in the

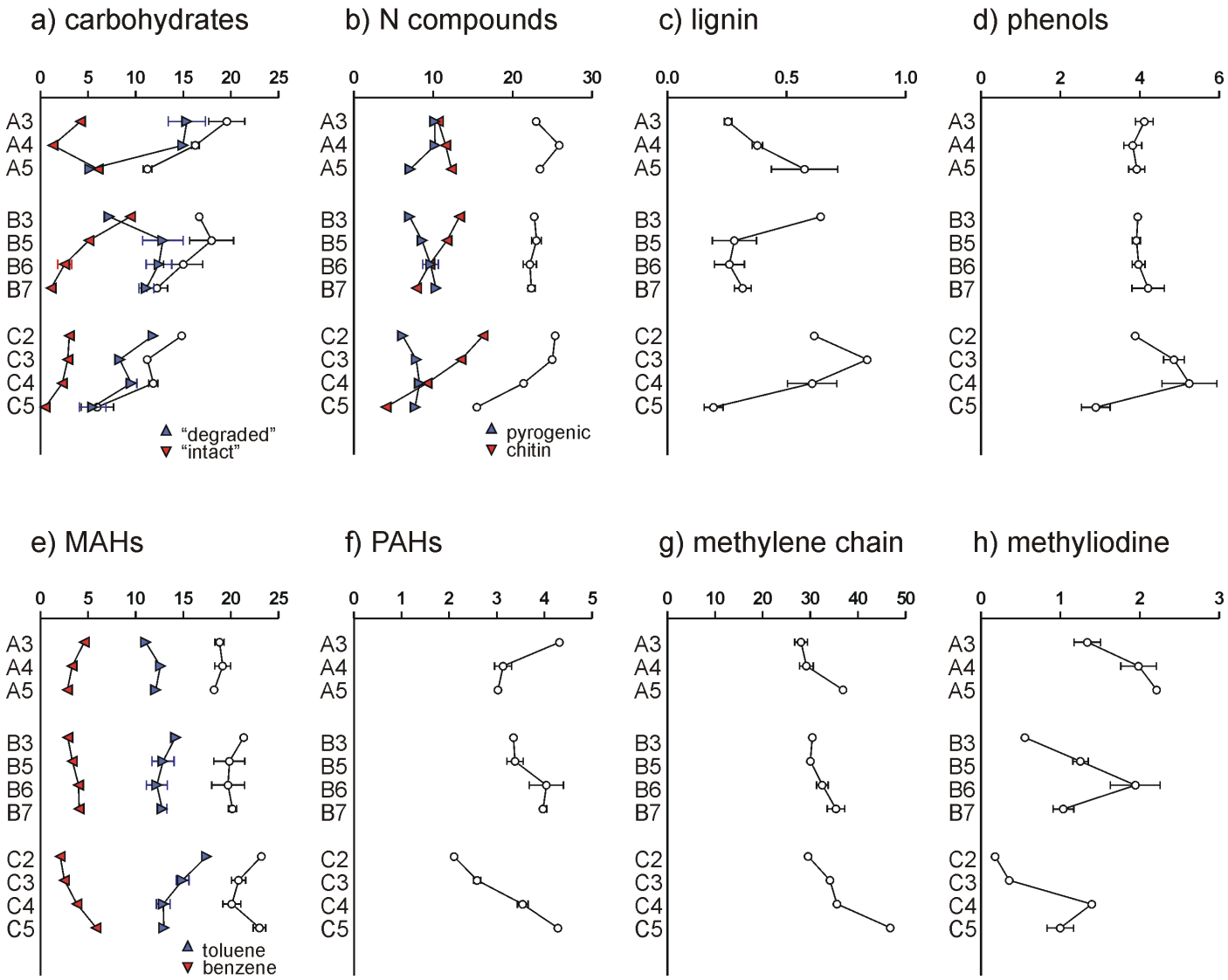

Fig. 4. Relative proportions of the different groups of pyrolysis products. Sum of total compounds in group in white symbols, subgroups are indicated for carbohydrates, N-compounds and MAHs (monocyclic aromatic hydrocarbons).

initial scannings of the pyrograms, showed that it is correlated to Me-I (r^2=0.72, P<0.001), with the relative proportion of Me-I and Me-Br being roughly 4:1. Other compounds detected are an aliphatic pyrolysis product with characteristic fragment ions m/z 83 and 280, frequently associated with fresh plant remains, and an unidentified polar compound with base ion m/z 135 (possibly from chitin).

B. Coupling of Py-GC-MS fingerprints and geo-archaeological information

It appeared that the SOM of the soils studied is a mixture of relatively intact plant-derived "labile" SOM (polysaccharides and lignin), aliphatic "recalcitrant" SOM (C_{10}-C_{25} alkane/alkene pairs), "degraded/secondary" SOM (furfurals, chitin markers) and pyrogenic SOM (benzene, PAHs, benzonitriles, naphthalene carbonitriles), in varying relative proportions. Figure 5 shows the relative proportions of these groups, omitting all compounds of unspecific origin. It seems that the majority of the SOM originates from biotically (microbially or arthropodically) altered SOM (degraded/secondary SOM) and aliphatic "recalcitrant" SOM. This can be explained by the intensity of SOM degradation, eliminating most plant-derived labile components leaving the degraded/secondary (e.g. chitin) and recalcitrant SOM. Preferential decomposition of chitin may explain the relative increase in the proportions of pyrogenic and recalcitrant SOM with depth (profiles B and C). Note that these are only rough estimations that may be severely biased (e.g. because of low pyrolysability of pyrogenic matter).

Profile A. Sample A5 corresponds to the Early Holocene (a post-glacial deposit ca. 14 ka old) and therefore contains no or very few fire residues. The fire regime had not started yet and the SOM is composed predominantly of recalcitrant aliphatic domains (from roots for example). Sample A4 is deep black in colour and has larger microbial and pyrogenic SOM contents. This corroborates the abundance macroscopic charcoal and suggests that the "black particles" mentioned by Mailänder et al. (2010) (referring to sample A4) indeed originate from fire residues, presumably from anthropogenic fire clearance during the Neolithic (upper and lower boundaries dated to 6000 and 6500 cal BP, respectively). Sample A3 (4500 cal BP) is an exception to the rule that the dark-coloured samples have highest Black C contents. It has a reddish colour and is clearly post-Neolithic. This may be related to its low C content (weak pigmenting effect of pyrogenic SOM) and/or the presence of Black C at the lower boundary between A3 and A4.

In profile B, a clear increase in pyrogenic SOM content is observed, culminating into the darkest levels that were dated to 6500 cal BP. Surface levels of profile B have a relatively high proportion of well-preserved plant remains.

A similar pattern is recognised in profile C. The youngest samples analysed here date to 1200 cal BP (sample C2, ca. 800 A.D.) and is a greyish layer that was formed well after the dark-coloured layers that formed more than 1000 years earlier (C3, 2500 cal BP). Sample C2 has no or very little pyrogenic SOM, whereas C3 has slightly higher levels. The highest proportion of pyrolysis products of Black C are found in samples C4 (not dated) and C5 (7000 cal BP), which are also deep black in colour.

4. CONCLUSIONS

The geo-archaeological survey already showed clear consistency in the depth-age records and determined age of the dark-coloured deeper layers: they correspond to a rather narrow age range between 6000 and 7000 years ago, corresponding to Neolithic fire events. It has now been established on the basis of molecular data that the black colour of these layers can indeed be safely ascribed to the abundance of Black C, i.e. fire residues. Clearly, considering their thickness, these dark layers correspond to a very intense recurrent fire regime. Early human-induced anthropogenic erosion processes could thus be dated as far back as the early Neolithic. According to Mailänder et al. (2010) it was probably caused by vegetation clearance and initial slash and burn agriculture. The abrupt shift in lighter materials after the Neolithic can be related to the absence of biomass (fuel) after deforestation: post-Neolithic sporadic burning of herbaceous vegetation in pasturelands or elimination of weeds from a fully converted agricultural landscape, of which evidence exists near Ipf, would not give rise to deep-black charcoal-rich colluvium.

5. REFERENCES

Kaal, J., Nierop, K.G.J., Martínez Cortizas, A., 2009. Characterisation of aged charcoal using a coil probe pyrolysis-GC/MS method optimised for Black Carbon. Journal of Analytical and Applied Pyrolysis 85, 408-416.

Kaal, J., Rumpel, C., 2009. Can pyrolysis-GC/MS be used to estimate the degree of thermal alteration of black carbon? Organic Geochemistry 40, 1179-1187

Knicker, H., 2010. "Black nitrogen" - an important fraction in determining the recalcitrance of charcoal. Organic Geochemistry 41, 947-950.

Mailänder, S. Eberle, J., Blümel, W.D., 2010. Kolluvien, Auelehme und (An)moore im Umfeld des frühkeltischen Fürstensitzes auf dem Ipf – Ein Beitrag zur Geoarchäologie und Landschaftsgeschichte am Westrand des Nördlinger Rieses. In: Krausse, D.L., 2010, Frühe Zentralisierungs- und Urbanisierungsprozesse. Zur Genese und Entwicklung frühkeltischer Fürstensitze und ihres territorialen Umlandes. Kolloquium des DFG-Schwerpunktprogramms 1171.

Mailänder, S., Hecht, S., Eberle, J., Blümel, W.D., 2011. Geoarchäologische Erkundungen in zwei Muldentälchen östlich des Ipfs am Westrand des Nördlinger Rieses (Süddeutschland). Tagungen des Landesmuseum für Vorgeschichte Halle, Band 6, 129-144.

Martínez Cortizas, A., Ferro Vázquez, C., Kaal, J., Biester, H., Costa Casais, M., Taboada Rodríguez, T., Rodríguez Lado, L., 2016. Bromine accumulation in acidic black colluvial soils. Geochimica et Cosmochimica Acta 174, 143-155.

Schellekens, J., Buurman, P., Fraga, I., Martínez-Cortizas, A., 2011. Holocene vegetation and hydrologic changes inferred from molecular vegetation markers in peat, Penido Vello (Galicia, Spain). Palaeogeography, Palaeoclimatology, Palaeoecology 299, 55-69.

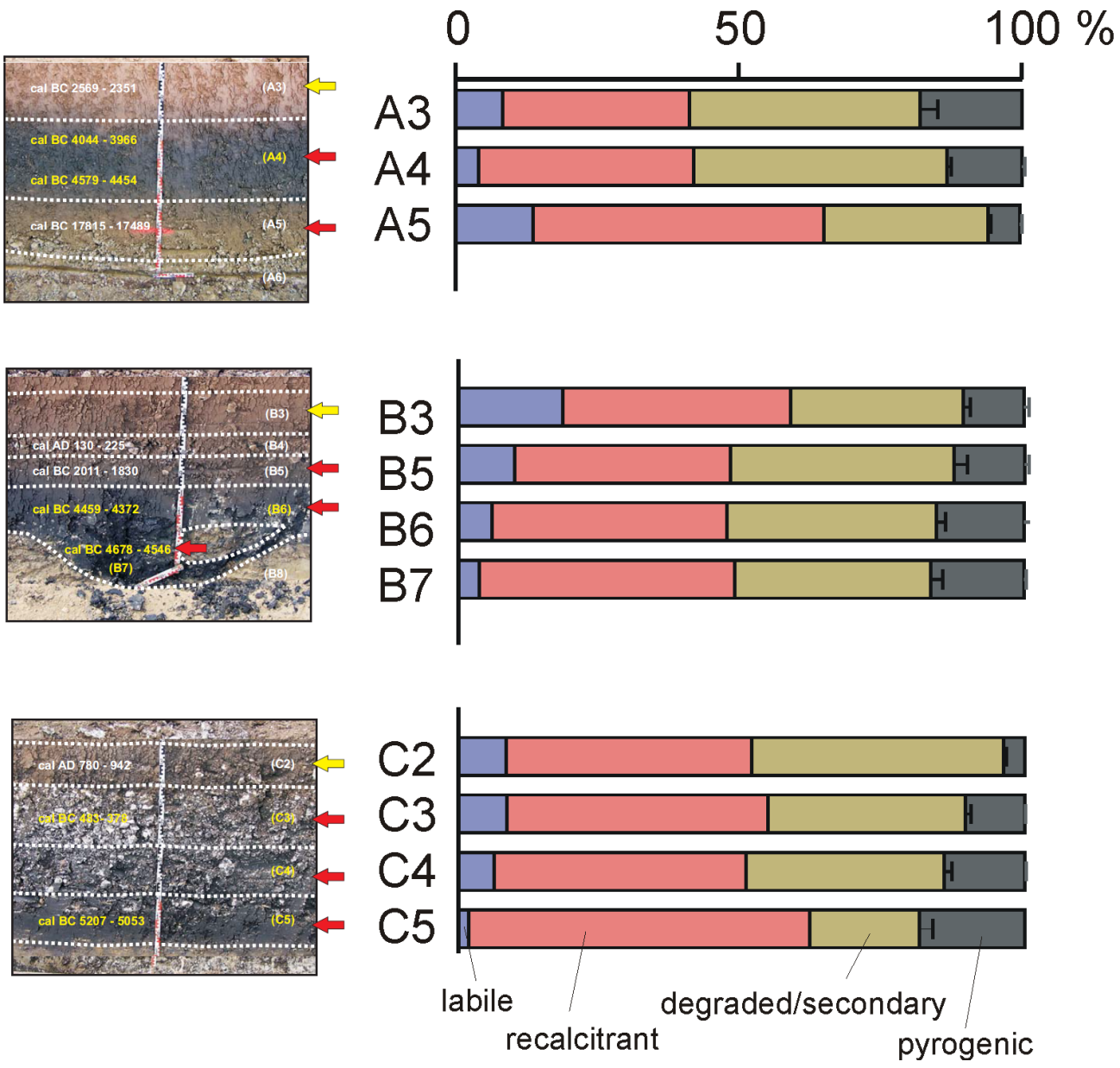

Fig. 5. Relative proportions of labile plant-derived SOM, microbial SOM, recalcitrant aliphatic SOM and pyrogenic SOM

Table 1. List of pyrolysis products and source allocation (CARB=carbohydrate, LIG=lignin, MAH=monocyclic aromatic hydrocarbon, MCC=methylene chain compound, NCOMP=N-compound, PAH=polycyclic aromatic hydrocarbon, PHEN=phenol)

Label	RT (min)	Compound	m/z	group
1	1.689	I-methane	142+127	OTHER
2	2.145	benzene	78	MAH
3	2.809	toluene	91+92	MAH
4	3.593	xylenes (2 isomers)	91+106	MAH
5	3.894	4-ethylbenzene	91+106	MAH
6	3.878	styrene	104+78	MAH
7	6.447	naphthalene	128	PAH
8	7.272	C1-naphthalene	142+115	PAH
9	7.401	C1-naphthalene	142+115	PAH
10	5.253	indene	115+116	PAH
11	6.130	C1-indene	130+115	PAH
12	7.832	biphenyl	154+153	PAH
13	8.019	C2-naphthalene (2 isomers)	156+141	PAH
14	8.787	dibenzofuran	168+139	PAH
15	9.197	fluorene	165+166	PAH
16	10.385	phenanthrene	178	PAH
17	4.984	phenol	94+66	PHEN
18	5.539	C1-phenol (2 isomers)	108+107	PHEN
19	6.250	C2-phenol	107+122	PHEN
20	5.684	guaiacol	109+124	LIG
21	7.401	4-vinylguaiacol	150+135	LIG
22	3.370	3/2-furaldehyde	95+96	CARB
23	4.594	5-methyl-2-furaldehyde	110+109	CARB
24	5.004	pyran comp	114+58	CARB
25	5.352	dianhydrorhamnose	128+113	CARB
26	5.918	levoglucosenone	68+98	CARB
27	8.958	unidentified carbohydrate	116	CARB
28	9.321	levoglucosan	60+73	CARB
29	2.612	N-methylpyrrole	81+80	NCOMP
30	2.727	pyridine	79+52	NCOMP
31	2.768	pyrrole	67	NCOMP
32	3.307	C1-pyridine	93+66	NCOMP
33	3.546	C1-pyrrole (2 isomers)	80+81	NCOMP
34	3.800	acetamide	59	NCOMP
35	4.807	benzonitrile	103+76	NCOMP
36	4.999	unidentified N-compound	109	NCOMP
37	6.032	benzeneacetonitrile	117+90	NCOMP

Continued on next page

Continued from previous page

Label	RT (min)	Compound	m/z	group
38	6.110	C1-benzonitrile	117+90	NCOMP
39	7.373	indole	117+90	NCOMP
40	8.716	naphthalene carbonitrile	153+126	NCOMP
41	8.823	phthalimide	147+76	NCOMP
42	8.870	trianhydro-2-acetamido-2-deoxyglucose	125+167	NCOMP
43	8.906	naphthalene carbonitrile	153+126	NCOMP
44	9.186	unidentified N-compound	94	NCOMP
45	9.285	C1-phthalimide	161	NCOMP
46	9.550	C1-phthalimide	161	NCOMP
47	10.011	diketodipyrrole	186+93	NCOMP
48	10.748	C16 alkylnitrile	97+110	NCOMP
49	11.303	2,5-diketopiperazine	70+194	NCOMP
50	11.734	C18 alkylnitrile	97+110	NCOMP
51	12.175	C16 alkylamide	59+72	NCOMP
52	13.041	C18 alkylamide	59+72	NCOMP
53	7.505	unidentified compound	135+165	OTHER
54	12.787	unidentified compound	83+280	OTHER
55	15.807	steroid/triterpenoid	396+147	OTHER
56	4.693	C10-alkene	55+69	MCC
57	4.760	C10-alkane	57+71	MCC
58	5.518	C11-alkene	55+69	MCC
59	5.596	C11-alkane	57+71	MCC
60	6.312	C12-alkene	55+69	MCC
61	6.369	C12-alkane	57+71	MCC
62	7.038	C13-alkene	55+69	MCC
63	7.090	C13-alkane	57+71	MCC
64	7.733	C14-alkene	55+69	MCC
65	7.775	C14-alkane	57+71	MCC
66	8.392	C15-alkene	55+69	MCC
67	8.413	C15-alkane	57+71	MCC
68	8.989	C16-alkene	55+69	MCC
69	9.031	C16-alkane	57+71	MCC
70	9.586	C17-alkene	55+69	MCC
71	9.601	C17-alkane	57+71	MCC
72	9.783	prist-1-ene	55+56	MCC
73	10.115	C18-alkene	55+69	MCC
74	10.151	C18-alkane	57+71	MCC
75	10.644	C19-alkene	55+69	MCC
76	10.681	C19-alkane	57+71	MCC

Continued on next page

Continued from previous page

Label	RT (min)	Compound	m/z	group
77	11.137	C20-alkene	55+69	MCC
78	11.137	C16 fatty acid	60+73	MCC
79	11.142	C20-alkane	57+71	MCC
80	11.635	C21-alkene	55+69	MCC
81	11.651	C21-alkane	57+71	MCC
82	12.030	C22-alkene	55+69	MCC
83	12.030	C18 fatty acid	60+73	MCC
84	12.092	C22-alkane	57+71	MCC
85	12.491	C23-alkene	55+69	MCC
86	12.528	C23-alkane	57+71	MCC
87	12.922	C24-alkene	55+69	MCC
88	12.948	C24-alkane	57+71	MCC
89	13.332	C25-alkene	55+69	MCC
90	13.342	C25-alkane	57+71	MCC
91	13.711	C26-alkene	55+69	MCC
92	13.716	C26-alkane	57+71	MCC
93	14.090	C27-alkene	55+69	MCC
94	14.090	C27-alkane	57+71	MCC
95	14.183	methylketone	58+59	MCC
96	14.442	C28-alkane	57+71	MCC
97	14.448	C28-alkene	55+69	MCC
98	14.795	C29-alkane	57+71	MCC
99	14.904	methylketone	58+59	MCC
100	15.127	C30-alkane	57+71	MCC
101	15.132	C29-alkene	55+69	MCC
102	15.496	C30-alkene	55+69	MCC
103	15.501	C31-alkane	57+71	MCC
104	15.605	methylketone	58+59	MCC
105	15.869	C31-alkene	55+69	MCC
106	15.874	C32-alkane	57+71	MCC
107	16.295	C33-alkane	57+71	MCC
108	16.456	methylketone	58+59	MCC